

Unsupervised Pretraining for Object Detection by Patch Reidentification

Jian Ding^{1*}, Enze Xie^{3*}, Hang Xu², Chenhan Jiang², Zhenguo Li², Ping Luo³, Gui-Song Xia¹

¹Wuhan University, ²Huawei Noah's Ark Lab, ³The University of Hong Kong

Abstract

Unsupervised representation learning achieves promising performances in pre-training representations for object detectors. However, previous approaches are mainly designed for image-level classification, leading to suboptimal detection performance. To bridge the performance gap, this work proposes a simple yet effective representation learning method for object detection, named patch re-identification (Re-ID), which can be treated as a contrastive pretext task to learn location-discriminative representation unsupervisedly, possessing appealing advantages compared to its counterparts. **Firstly**, unlike fully-supervised person Re-ID that matches a human identity in different camera views, patch Re-ID treats an important patch as a pseudo identity and contrastively learns its correspondence in two different image views, where the pseudo identity has different translations and transformations, enabling to learn discriminative features for object detection. **Secondly**, patch Re-ID is performed in **Deeply Unsupervised** manner to learn multi-level representations, appealing to object detection. **Thirdly**, extensive experiments show that our method significantly outperforms its counterparts on COCO in all settings, such as different training iterations and data percentages. For example, Mask R-CNN initialized with our representation surpasses MoCo v2 and even its fully-supervised counterparts in all setups of training iterations (e.g. 2.1 and 1.1 mAP improvement compared to MoCo v2 in 12k and 90k iterations respectively). Code will be released at <https://github.com/dingjiansw101/DUPR>.

1. Introduction

Pre-training representation is important for object detection, as training object detectors from scratch is very hard, especially for small datasets, and it has been dominated by supervised training on ImageNet for a long time [12, 33, 26]. However, the annotation of a large-scale dataset is time-consuming and expensive, and preparing such a dataset for each task is impractical. Alternatively, unsupervised visual representation learning aims at

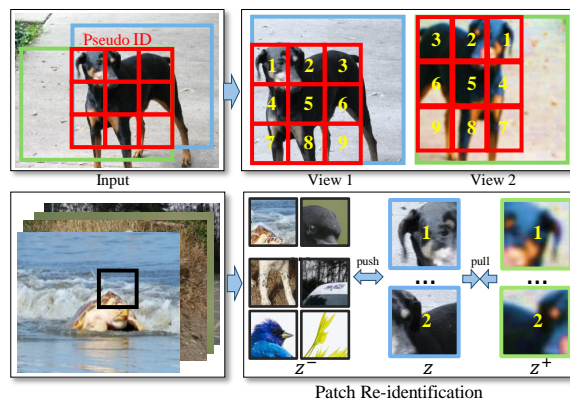


Figure 1. Illustration of unsupervised pre-training visual representation for object detection by patch Re-ID, which follows the merits of person Re-ID that matches a human identity between cameras. In patch Re-ID, the intersection area (red bounding box) of two views is treated as a pseudo identity, and the unsupervised features are learned by matching the patches at the same position (denoted by number) of pseudo ID in two views (e.g. blue and green boxes), where the pseudo ID can be presented with different translations and transformations (e.g. flipping and color jittering), making the learned representations sensitive to spatial positions, which is important for object detection.

pre-training models without human annotations and then transferring the features to downstream tasks by finetuning, which allows us to pre-train models with plenty of unlabeled data for free [17, 2, 9, 13, 41, 21].

Many unsupervised learning algorithms design pretext tasks to train deep neural networks, such as the rotation prediction task [11], jigsaw [30], relative location prediction [7] and combination of multi-task [8], etc. Although promising results have been reported, representations pre-trained from these pretext tasks still have a large performance gap to the ImageNet supervised counterpart. Meanwhile, recent contrastive learning-based methods have achieved great success [17, 4, 36, 31, 34, 16]. Some pretext tasks can be based on contrastive loss function. For example, the representative MoCo [17] and SimCLR [4] use instance discrimination task, which considers an image and its transformations as the same class and other images as different class. This task learns representations which are discriminative across different images and invariant to transformations. Although methods like MoCo [17] bridge the

*Equal contribution

gap with the supervised counterpart in linear evaluation on ImageNet, the designs are suboptimal for object detection. Since these methods also learn a *spatial invariant* feature by considering two images with objects at different locations (in image) as positive pairs, and there is a dilemma of increasing *spatial invariance* for classification vs. respecting *spatial sensitivity* for localization as demonstrated in [6]. Moreover, previous works focus on learning discriminative features at the final layer (e.g., on the $32\times$ feature map) [17, 4], while most deep learning-based object detectors need to extract features from the multi-level representation [25, 27]. Thus, it is important to have discriminative features at different feature layers instead of only the final one on pyramids.

To address the aforementioned problems, we propose to pre-train spatial sensitive representations for object detection by *Deeply Unsupervised Patch Re-ID (DUPR)*. The target of *patch Re-ID* is to identify patches of the same identity at the corresponding position in two synthesis views generated by random transformations. As we do not have ground truth bounding box of the object, we use the intersection area between two views as pseudo identity. Then we split the intersection box as $S \times S$ patches and learn to match the same positions between two views. The features of matched patches should be more similar than unmatched patches. Our patch Re-ID is a pretext task and independent of the detailed loss function, so we simply adopt the InfoNCE [31] in this work. By minimizing the patch contrastive loss, encoder can learn spatial sensitive features to benefit object detection. Furthermore, we propose a *deeply unsupervised training strategy* to learn multi-level representations. Specifically, we extract features from different intermediate layers to construct both image and patch-level contrastive loss.

Our contributions can be summarized as follows:

- We propose a *patch Re-ID* pretext task which learns to identify the patches with the same position between two views and capture more spatial information, which is important for object detection.
- We present the deep unsupervised training strategy to train multi-level feature maps in an unsupervised style to improve the transferability of object detectors.
- Our pre-trained model outperforms other self-supervised models and supervised counterparts when transferring to object detection across several datasets and object detectors. For example, when finetuning Mask R-CNN R-50-FPN on COCO, DUPR outperforms all other unsupervised and supervised models at different iterations as shown in Fig. 2.

2. Related Work

Self-supervised learning. Self-supervised learning leverages input data itself as supervision via pretext tasks. After

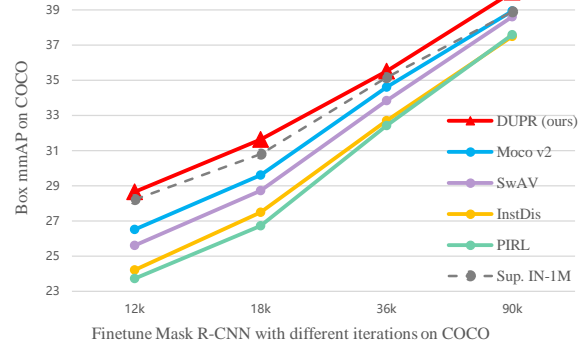


Figure 2. **Finetuning Mask R-CNN R-50-FPN on COCO with different iterations.** All the reported unsupervised models are pre-trained on the ImageNet-1M training set with 200 epochs. DUPR outperforms all other unsupervised methods and even the supervised counterpart at all iterations. When finetuning Mask R-CNN with 12k iterations, DUPR outperforms the MoCo v2 by 2 points in mAP.

training in pretext task, the features are transferred to downstream tasks. Such as rotation prediction [11], relative loc prediction [7], jigsaw [30] and colorization [38, 39], etc. These methods achieve promising results but still have a large gap compared to supervised pre-training. Recently, the most successful method in self-supervised learning is contrastive learning [15] via instance discrimination pretext task. The main idea of contrastive learning is to pull together similar image pairs while pushing apart dissimilar pairs. The success of contrastive learning is related to the maximization of mutual information between latent representations of two views [31]. Different pretext tasks choose different views to maximize their mutual information. For example, CPC [31] and CPC v2 [20] take the context and future as two views. Deep infomax [22] and AMIDIM [1] take the global and local feature as two views, while the MoCo [17] and SimCLR [4] take the global features as two views. All these methods considered the images with objects at different location as positive pairs to learn a spatial invariant representation. Unlike these methods, we consider the spatial position as shared information. The patches at the same location in two views are positive pairs, which can capture more spatial information.

Deep Supervision. Deep supervision proposed in the deeply supervised network (DSN) [24] acts as a kind of regularization and speeds up the convergence of the supervised network. It has also been used in HED [37] and PSPNet [40] for hierarchical edge detection and semantic segmentation. In our work, we aim at learning more discriminative shallow features to facilitate the transferring to object detection, so we propose the deeply unsupervised training strategy in an end to end way.

Object Detection. The task of object detection is to locate objects in images and classify their categories. Being different from classification, which is image-level prediction

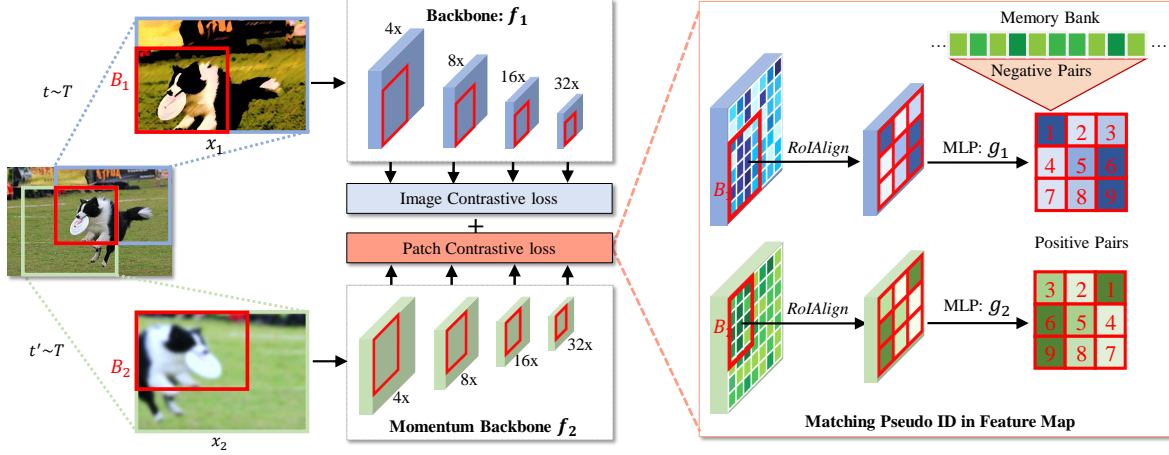


Figure 3. **The pipeline of Deeply Unsupervised Patch Re-ID (DUPR).** The original image x is augmented into two views x_1 and x_2 . The blue and green bounding box correspond to the original area of x_1 and x_2 , respectively. The red bounding box is the intersection area. x_1 and x_2 are passed to the backbone and momentum backbone, respectively. We take four feature levels to construct the contrastive loss. Each feature level includes an image-level contrastive loss and a patch-level contrastive loss. The patch Re-ID is designed to match the corresponding patches at the same position (denoted by the number in the figure) between two views. We first extract the intersection features through RoI Align. Then each RoI feature is split into $S \times S$ patches. The patch contrastive loss makes feature sensitive to spatial changes, contributing to the localization task.

task, object detection is region-level prediction task. For two-stage object detectors [33, 18], region features are extracted from the proposals (generated by selective search or RPN [33]) by RoI Align [18]. For one-stage object detectors [28, 32, 26, 35], region features are extracted from sliding windows. For each region, the localization prediction is usually encoded as position offset relative to the anchor. If a region has a high IoU with the ground truth bounding box, it should have higher confidence for category prediction and smaller offset prediction. So the region features should be sensitive to the spatial position to get accurate bounding box prediction. Object detection also requires multi-level representations, as predictions are directly made by using multi-level features [28], or the fusion of multi-level feature maps [25, 27]. Our work focuses on learning discriminative region-level features from multiple layers to pre-train suitable representations for object detection.

3. Method

3.1. Preliminary: Contrastive Learning

In this section, we illustrate the contrastive learning [17, 4, 36] from the view of Re-ID. The contrastive learning can be considered as a Re-ID task, where features of two images sharing the same identity but should be similar in different views. In particular, for person/vehicle Re-ID, suppose one person/car under different cameras with different viewpoints, poses and lighting conditions, they **naturally** have different views. For self-supervised Re-ID, suppose x is original image, x_1 and x_2 can be considered as two synthetic views of the same identity with different **artificially** augmentations. Denote v_1 and $v_{2,+}$ to be the normalized

embedding of x_1 and x_2 . The target of contrastive learning is to pull together positive pairs $(v_1, v_{2,+})$ while push apart negative pairs $(v_1, v_{2,j})$. The conventional learning objective is the InfoNCE [31] loss:

$$\mathcal{L}_{v_1, v_{2,+}} = -\log \frac{\exp(v_1 \cdot v_{2,+} / \tau)}{\sum_{j=0}^K \exp(v_1 \cdot v_{2,j} / \tau)}. \quad (1)$$

Here τ is a temperature hyper-parameter. $v_1 \cdot v_{2,j}$ is the cosine similarity to measure the distance between two image features. It can be considered as a non-parametric softmax-based classifier to identify v_1 as $v_{2,+}$. According to different selections of views, v_1 and $v_{2,+}$ can be pairs of global-local features [1, 22] or global-global features [17, 4]. All these pretext tasks mainly focus on category discrimination but do not care about the object's location.

3.2. Deeply Unsupervised Patch ReID

To learn a spatial sensitive feature, we design the patch Re-ID as a pretext task, which can train an encoder to re-identify the corresponding patches of two views, as shown in Fig. 3. We also perform image-level contrastive learning to increase the classification ability. Since most object detectors need a multi-level representation, we propose a deeply unsupervised training strategy. More specifically, we add image and patch-level contrastive loss for each layer. The overall loss is defined as:

$$\mathcal{L} = \sum_{m=0}^M \alpha_m \mathcal{L}_g^{(m)} + \sum_{m=0}^M \beta_m \mathcal{L}_p^{(m)} \quad (2)$$

where M is the number of feature maps we use. $\mathcal{L}_g^{(m)}$ and $\mathcal{L}_p^{(m)}$ are the image and patch contrastive loss for feature

map of m -th level. α_m and β_m are the weights to balance the importance of different levels. We will describe the details in the following.

Multi-Level Feature Extraction. We extract feature maps from multiple layers, as shown in Fig. 3. First, the original image x is transformed into two views x_1 and x_2 via random augmentations, including color jitter, gaussian blur, random flip, grayscale, and random resized crop. Then these two augmented images are fed into the backbone and momentum backbone, respectively. For each backbone, we extract feature pyramids at different resolutions. Let $f_1^{(m)}(x_1)$ and $f_2^{(m)}(x_2)$ denote the features from the m -th feature map of backbone and momentum backbone. We add the image and patch-level contrastive loss to different feature map levels since most object detectors require multi-level representations.

Patch Re-ID. This is a pretext task to perform patch-level matching of the same identity between two views. We first create two views via augmentations, as shown in Fig. 3. The ideal target is to match the ground truth bounding boxes of the same identity in two synthesis views. However, in an unsupervised setting, we do not have ground truth. Therefore, we consider the intersection area as a pseudo bounding box of identity (the red box in Fig. 3). Instead of using a global averaged feature from the bounding box of pseudo identity, which loses spatial information, we split the intersection bounding box into $S \times S$ patches and maximize the similarity between the corresponding patch features. The process is shown in Fig. 3, where the augmented images x_1 and x_2 correspond to the blue bounding box and the green one in original image x . The red bounding box is the intersection area of two views. We denote the intersection bounding box in the coordinates of x_1 and x_2 as \mathcal{B}_1 and \mathcal{B}_2 . Note both position and size of \mathcal{B}_1 and \mathcal{B}_2 are different. For the m -th feature map, we apply RoI Align [18] to extract region feature followed by a pixel-wise MLP layer which is implemented by a 1×1 convolution as:

$$r_1^{(m)} = g_1^{(m)}(\text{RoIAlign}(f_1^{(m)}(x_1), \mathcal{B}_1)) \quad (3)$$

$$r_2^{(m)} = g_2^{(m)}(\text{RoIAlign}(f_2^{(m)}(x_2), \mathcal{B}_2)) \quad (4)$$

where $g_1^{(m)}$ and $g_2^{(m)}$ are MLP layer and momentum MLP layer respectively. $r_1^{(m)}$ and $r_2^{(m)}$ are region feature maps of a fixed shape (C, S, S) . Then $r_{1,ij}^{(m)}$ and $r_{2,ij}^{(m)}$ is positive pair, where the subscript $(i, j) \in [0, S) \times [0, S)$ denotes the position in the region. Although our patch Re-ID pretext task is independent of loss function, we simply adopt the InfoNCE [31] loss and follow [17] to use a dynamic memory bank to store features from momentum updated encoder. We construct the patch contrastive loss for the m -th feature

map as:

$$\mathcal{L}_p^{(m)} = - \sum_{i,j} \log \frac{\exp(r_{1,ij}^{(m)} \cdot r_{2,ij}^{(m)} / \tau)}{\exp(r_{1,ij}^{(m)} \cdot r_{2,ij}^{(m)} / \tau) + \sum_{t=1}^K \exp(r_{1,ij}^{(m)} \cdot r_t^{(m)} / \tau)} \quad (5)$$

where $\{r_t^{(m)}\}_{t=1,\dots,K}$ are patch features of other images from memory bank. m denotes the index of feature map. By minimizing the patch contrastive loss, our encoder can learn patch-wise matching of identity between two views. Such matching ability results in spatial sensitive features, which facilitate object detection.

Image-Level Contrastive Loss. We also optimize the image-level contrastive loss as it is important to improve the classification ability, which is also required by object detection. Denote $v_1^{(m)} = \text{avgpool}(f_1^{(m)}(x_1))$ and $v_{2,+}^{(m)} = \text{avgpool}(f_2^{(m)}(x_2))$ to be the normalized image features of positive pairs. For simplicity, we neglect the notation of normalization. The image-level contrastive loss for the m -th feature map can be written as:

$$\mathcal{L}_g^{(m)} = - \log \frac{\exp(v_1^{(m)} \cdot v_{2,+}^{(m)} / \tau)}{\sum_{j=0}^K \exp(v_1^{(m)} \cdot v_{2,j}^{(m)} / \tau)} \quad (6)$$

Mutual Information Discussion. It has been shown that optimizing the InfoNCE loss is equivalent to maximizing a lower bound on the mutual information [31] between $f_1(x_1)$ and $f_2(x_2)$:

$$I(f_1(x_1); f_2(x_2)) \geq \log(K) - \mathcal{L}_{NCE} \quad (7)$$

where \mathcal{L}_{NCE} is the expectation of $\mathcal{L}_{v_1, v_{2,+}}$ in Eq. (1).

The previous works are designed for classification by selecting views sharing the category. Optimizing the InfoNCE loss will maximize the mutual information $I(f_1(x_1); y)$, which is to maximize the shared information between the encoded feature $f_1(x_1)$ of x_1 and the label y of x_1 . However, the spatial information between them is not shared. In this case, encoder may discard the spatial information which is important for object detection.

In contrast, for patch Re-ID, a relative spatial position (e.g. top left, middle or bottom right of an object) is the shared information and related to the *localization of object*, leading to *better representation for object detection*. Note, our encoded *relative position* is different to the *absolute position* in [23]. The absolute position (coordinates) is independent of the content of images. Giving each pixel's absolute coordinates do not directly know how good an RoI overlaps the object. In contrast, our encoded relative position is correlated to the objects. Intuitively, identifying all relative spatial positions enables us to locate the entire bounding box of an object.

Here we present a rigorous illustration. As shown in Fig. 4, let p index different parts of an object, e.g. $p = 1$ and $p = 9$ indicate the top-left and bottom-right patches

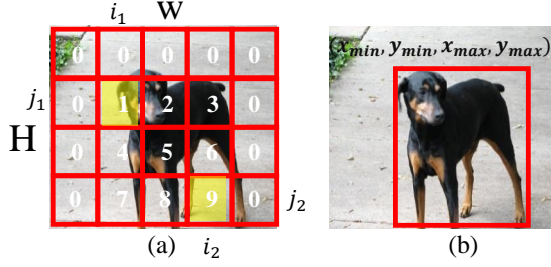


Figure 4. **Relation between object parts and bounding box encoding.** (a) The number p denotes a specific part of an object. For example, $p = 1$ and $p = 9$ denote the top left and bottom right of an object. (b) The bounding box of an object, where (x_{min}, y_{min}) and (x_{max}, y_{max}) denote the top left coordinate and bottom right coordinate of an object.

respectively. By optimizing \mathcal{L}_p in Eq.(5), we essentially maximize the mutual information $I(r_{1,i,j}; p)$, where $r_{1,i,j}$ is the feature at position (i, j) in Eq.(5). If the representation encodes more information of relative spatial position, it will capture more information of object bounding box, because we can obtain the object bounding box $(x_{min}, y_{min}, x_{max}, y_{max})$ from p as shown in Fig. 4. For example, we use (i_1, j_1) and (i_2, j_2) to denote the positions when $p = 1$ and $p = 9$. Then we can get the bounding box of an object by $(i_1 \times w, j_1 \times h, i_2 \times w, j_2 \times h)$, where w and h are the width and height of patches. As long as w and h are small, $(i_1 \times w, j_1 \times h, i_2 \times w, j_2 \times h)$ can approximate the true bounding box $(x_{min}, y_{min}, x_{max}, y_{max})$.

Implementation Details. We use unlabelled ImageNet as pre-training dataset for most of our experiments. For data augmentation, we follow the settings in [5]. We choose ResNet 50 [19] as our backbone and extract multi-level features from conv2_x, conv3_x, conv4_x and conv5_x. The stride of each feature map is $\{4 \times, 8 \times, 16 \times, 32 \times\}$ respectively. By default, we set $\alpha_{0:3} = (0.1, 0.4, 0.7, 1.0)$ and $\beta_{0:3} = (0, 0, 1, 1)$ for Eq. 2. The RoI sizes of patch features on conv5_x and conv4_x are 14 and 7 respectively. τ is 0.2 for both Eq. 5 and Eq. 6. We use a unique memory bank for each image and patch feature to keep the consistency between positive and negative examples. We store 65536 keys for each memory bank. For patch features, there are $S \times S$ features for a single level on a single image. When conducting the enqueue and dequeue operation, we sample 4 patch features to enqueue to prevent the memory bank from changing too fast, which may cause an inconsistency problem. Unless other specified, we train with a batch size of 256 for 200 epochs. We use a learning rate of 0.06 with a cosine decay schedule. The transferring experiments for all object detectors are implemented in detectron2¹. Following the settings in [17], we add an extra normalization layer for FPN.

¹<https://github.com/facebookresearch/detectron2>

$\alpha_{0:3}$	AP	AP ₅₀	AP ₇₅
(0,0,0,1)	57.0	82.4	63.6
(0,0,1,1)	57.4 (+0.4)	82.7 (+0.3)	64.1 (+0.5)
(1,1,1,1)	57.4 (+0.4)	82.3 (−0.1)	63.9 (+0.3)
(0.1,0.4,0.7,1)	57.6 (+0.6)	82.4 (+0.0)	64.2 (+0.6)

(a) Faster R-CNN, R50-C4

$\alpha_{0:3}$	conv1	conv2_x	conv3_x	conv4_x	conv5_x
(0,0,0,1)	29.1	47.3	58.8	74.0	84.1
(0,0,1,1)	29.4	47.6	60.0	81.0	83.7
(1,1,1,1)	30.8	57.2	70.5	80.3	82.9
(0.1,0.4,0.7,1)	29.6	52.1	68.8	80.9	83.7

(b) SVM Classification of Different Levels

Table 1. **Ablation of α_m for image contrastive loss.** All models are pre-trained with 200 epochs on ImageNet. α_m is the weight to balance each layer in Eq. 2. (a) Object detection is finetuned on Pascal VOC trainval07+12 and tested on the Pascal VOC test 2007. (b) The SVM classification is finetuned on Pascal VOC 2007. The results show that the classification performance of shallow layers is important when transferred to object detection.

4. Experimental Analysis

We first conduct experiments for hyperparameters then we demonstrate that our method outperforms other unsupervised learning methods and supervised counterparts in different settings and datasets when transferred to object detection. Finally, we analyze the properties of our learned features.

4.1. Ablation Experiments

Influence of $\alpha_{0:3}$ for Image Contrastive Loss. We explore the influence of α_m for each feature pyramid in Eq. 2. In ablation experiments, we set the learning rate as 0.03 and pre-train the model for 200 epochs. We finetune the Faster R-CNN R-50-C4 detector on Pascal VOC trainval07+12 for 24k iterations following the settings in MoCo [17]. The results in Tab. 1 (a) show that all configuration of α_m can improve the AP. By setting $\alpha_{0:3} = (0.1, 0.4, 0.7, 1.0)$, we achieve the best results in AP, and we use it by default in our experiments. Now we ablate the classification ability of intermediate layers. It can be seen in Tab. 1 (b) that all three configurations of $\alpha_{0:3}$ largely improve the classification performance of shallow layers. For example, when set $\alpha_{0:3} = (0.1, 0.4, 0.7, 1.0)$, it improves the classification performance of conv3_x by **10 points** and conv4_x by **6.3 points**. These results suggest that discriminative shallow layers are important when transferred to object detection. We also notice a decrease in the classification performance of the conv5_x, which makes sense as the optimization of multi-level contrastive loss is more challenging than single-level contrastive loss.

Influence of RoI Size. We add patch contrastive loss to conv5_x (by setting $\beta_{0:3} = (0, 0, 0, 1)$) and ablate the RoI size. Results in Tab. 2 (a) show that large RoI size improves the performance, which indicates that large RoI size can capture more precise spatial information, as discussed

$\alpha_{0:3}$	$\beta_{0:3}$	S	AP	AP ₅₀	AP ₇₅
(0.1,0.4,0.7,1)	(0,0,0,1)	3	58.1	82.5	65.0
(0.1,0.4,0.7,1)	(0,0,0,1)	7	58.3	82.7	64.9

(a) Ablation of RoI Size

$\alpha_{0:3}$	$\beta_{0:3}$	VOC			COCO	
		AP	AP ₅₀	AP ₇₅	AP ^{bb}	AP ^{mk}
(0.1,0.4,0.7,1)	(0,0,0,0)	57.6	82.4	64.2	39.2	35.5
(0.1,0.4,0.7,1)	(0,0,0,1)	58.3	82.7	64.9	39.5	35.7
(0.1,0.4,0.7,1)	(0,0,1,1)	58.5	83.2	65.2	40.0	36.2

(b) Ablation of $\beta_{0:3}$

$\alpha_{0:3}$	$\beta_{0:3}$	VOC			COCO	
		AP	AP ₅₀	AP ₇₅	AP ^{bb}	AP ^{mk}
(0,0,0,1)	(0,0,0,0)	57.0	82.4	63.6	38.9	35.5
(0,0,0,0)	(0,0,0,1)	57.9	82.2	64.6	38.8	35.3

(c) Compare image and patch contrastive loss

Table 2. (a) **Ablation of RoI size.** Larger size of RoI has better results. We add patch loss to the conv5_x feature map to do the RoI size ablation study on Pascal VOC, Faster R-CNN, R-50-C4. (b) **Ablation of β_m .** We use RoI size of 7 and 14 for conv5_x and conv4_x feature maps, respectively. (c) We compare single image and patch contrastive loss on conv5_x.

in Sec. 3.2. So we set the RoI size of conv5_x to 7 and conv4_x to 14 by default.

Influence of $\beta_{0:3}$ for Patch Contrastive Loss. Simply adding patch loss to conv5_x (by setting $\beta_{0:3} = (0, 0, 0, 1)$) improves the AP by 0.7 points in VOC and 0.3 points in COCO. Adding patch loss to both conv4_x and conv5_x feature map further improves the AP by 0.5 points in COCO and 0.2 points in VOC as shown in Tab. 2 (b), which indicates that intermediate supervision and patch contrastive loss are complementary.

Compare image and patch contrastive loss. We compared the single image and patch contrastive loss in Tab. 2 (c). Patch contrastive loss improves the localization ability but slightly reduces the classification ability. For example, patch contrastive loss improves the AP₇₅ (which is more related to localization ability) by 1.0 points but reduces the AP₅₀ by 0.2. It also slightly reduces the COCO AP by 0.1 points, since classification ability is more important to COCO than VOC (note COCO has 80 categories while VOC has 20 categories). When combining both image and contrastive loss and achieve a balance between classification and localization as shown in the bottom line of Tab. 2 (b), we achieve the best performance.

4.2. Pascal VOC Object Detection

We finetune the Faster R-CNN R-50-C4 on Pascal VOC trainval07+12 and evaluate the results on Pascal VOC test2007. The results in Tab. 3 show that DUPR outperforms other unsupervised methods and supervised counterparts. Most unsupervised methods outperform the supervised counterpart in AP₇₅, which indicates that the supervised representation may lose much information irrelevant to classification. Our DUPR outperforms the MoCo v2 in

pre-train	AP	AP ₅₀	AP ₇₅
random init.	33.8	60.2	33.1
supervised	53.5	81.3	58.8
NPID++ [29]	52.3 (−1.2)	79.1 (−2.2)	56.9 (−1.9)
InstDis [36]	55.2 (+1.7)	80.9 (−0.4)	61.2 (+2.4)
PIRL [29]	55.5 (+2.0)	81.0 (−0.3)	61.3 (+2.5)
SwAV [3]	56.1 (+2.6)	82.6 (+1.3)	62.7 (+3.9)
BoWNet [10]	55.8 (+2.3)	81.3 (+0.0)	61.1 (+2.3)
MoCo [17]	55.9 (+2.4)	81.5 (+0.2)	62.6 (+3.8)
MoCo v2 [5]	57.0 (+3.5)	82.4 (+1.1)	63.6 (+4.8)
DUPR (ours)	58.5 (+5.0)	83.2 (+1.9)	65.2 (+6.4)

Table 3. **Object detection on PASCAL VOC.** All the methods are pre-trained for 200 epochs on ImageNet-1M. We finetune the Faster R-CNN R-50-C4 on Pascal VOC trainval07+12 and evaluate on test2007. We show the gap compared to the ImageNet supervised counterpart in brackets. Green and red mean the increases and decreases of at least 0.5 points. The results of random init, supervised, and MoCo v2 are from [17]. The results of NPID++ [29] and SwAV are from [3]. Other results are implemented by us. Our method outperforms the supervised counterpart by **5.0 points** and the MoCo v2 by **1.5 points**.

AP₇₅ by **1.6 points** and **0.8 points** in AP₅₀. It verifies that DUPR contains more spatial information than MoCo v2 and ImageNet supervised pre-training models.

4.3. COCO Object Detection and Segmentation

We compare the finetuning results of Mask R-CNN R-50-FPN, Mask R-CNN R-50-C4, and RetinaNet R-50-FPN with other unsupervised methods and ImageNet supervised counterparts, including both one-stage and two-stage detectors with different backbones. For Mask R-CNN R-50-FPN, we also compare the finetuned results with other methods at fewer iterations and limited annotations, which have more practical value.

Mask R-CNN R-50-FPN. For Mask R-CNN, R-50-FPN, 1× schedule, all unsupervised models do not surpass supervised counterpart except DUPR as shown in Tab. 9 (a). DUPR outperforms other unsupervised methods and the supervised counterpart by **1.1 points** in mAP. In 2× schedule, DUPR outperforms MoCo v2 by **0.7** in mAP and the supervised counterpart by **1.0** in mAP as shown in Tab. 9 (c).

Mask R-CNN R-50-C4. In 1× schedule, DUPR consistently outperforms all other unsupervised methods and the supervised counterpart by **1.4** in mAP as shown in Tab. 9 (b), which verifies that our method is robust to backbones. In 2× schedule where pre-training is less important, our method still outperforms the MoCo v2 by **0.3** in mAP as shown in Tab. 9 (d).

RetinaNet R-50-FPN. It is also important to have good transferability on one-stage object detectors. We choose to finetune the RetinaNet [26] with R-50-FPN on COCO in 1× and 2× schedule. As shown in Tab. 7, Instance Discrimination [36], PIRL [29], SwAV [3] are largely below the supervised models while MoCo v2 has the same AP as the

supervised counterpart. Our method outperforms all other unsupervised models and outperforms the supervised counterpart by **0.6** points in mAP.

Finetune with fewer iterations. We explore the performance of different unsupervised models at iterations of 12k, 18k, 36k, and 90k in Fig. 2. Our DUPR outperforms all other unsupervised models and even the supervised model pre-trained on ImageNet-1M at all iterations. When finetuning with only 12k iterations, DUPR outperforms the MoCo v2 by **2** points in mAP. It indicates that DUPR provides a better initialization and convergence faster than other methods. When finetuning with 90 iterations, DUPR outperforms the supervised counterpart by **1.1** points.

Finetune with limited annotations. The results are shown in Tab. 10. We randomly sample 1% and 10% annotations from COCO train2017 set and test on val2017 set. We finetune the Mask R-CNN R-50-FPN for 15k iterations on COCO 10% and 60k iterations on COCO 10%, respectively. When only use 1% annotations, our DUPR outperforms the MoCo v2 by 2.1 points. Note the mAP of MoCo v2 is below the ImageNet supervised counterpart by 2.2 points. When using 10% annotation for finetuning, our DUPR consistently outperforms the MoCo v2 and the supervised model by **1.3** points in mAP.

4.4. Instance seg. and semantic seg. on Cityscapes

Instance Segmentation. We finetune the Mask R-CNN R-50-FPN following [17]. DUPR outperforms MoCo v2 by **0.5** points in mAP as shown in Tab. 8.

Semantic Segmentation. Since there is no official code release, we reimplement the FCN-based structure following [17]. Our method outperforms MoCo v2 by **0.9** points as shown in Tab. 8. The results on cityscapes indicate that DUPR has good transferability to other localization sensitive tasks.

4.5. Performance on Classification

Object detection includes classification and localization. To better understand why DUPR improves object detection, we also report the classification results for reference to obtain more insight. We consider linear evaluation on ImageNet and Places365 and SVM classification on VOC. For ImageNet and VOC, we follow the standard settings. For Places365, we finetune the model by 56 epochs and report both the results from feat5 and unpool (see `openselfsup`² for more details). As can be shown in Tab. 4, DUPR has a drop of 3.7 in ImageNet linear evaluation. The classification drops are also noticed in VOC and Places365 except for the PL (unpool). *We can conclude that the improvements of DUPR in object detection is not from better clas-*

²<https://github.com/open-mmlab/OpenSelfSup>

pre-train	ImageNet cls.	VOC cls.	PL (feat5)	PL (unpool)
MoCo v2 [5]	67.5	84.1	49.4	46.6
DUPR	63.8	82.9	48.4	46.7

Table 4. **Performance on classification.** The ImageNet cls. means linear evaluation on ImageNet. VOC cls. means VOC SVM classification. PL denotes the Places365. Feat5 and unpool are features after and before averaged pooling.

pre-train	epoch	ImageNet cls.	COCO	VOC det.
BYOL [14]	300	74.3	37.5	51.9
MoCo v2 [5]	200	67.5	38.9	57.0
DUPR	200	63.8	39.6	58.5

Table 5. **Object detection v.s. Classification.** The ImageNet cls. means linear evaluation on ImageNet. For COCO and VOC detection, we report results of Mask R-CNN with R-50-C4 from Faster R-CNN with R-50-C4.

sification but the localization ability. We also notice an inconsistency between the object detection and classification performance for several different self-supervised learning methods in Tab. 5. These results make sense as there is an inconsistency between translation invariance in image classification and spatial sensitive in object localization [6]. The previous methods tend to learn a spatial invariant representation. On the contrary, the design of DUPR is to learn a spatial sensitive representation.

4.6. Pre-train Models on COCO

COCO dataset has a long-tailed, unbalanced distribution of real-world data and contains multiple objects in one image, while ImageNet dataset is clean with a balance category, usually containing only one object in an image. Almost all the previous methods use the ImageNet as pre-training dataset. However, unsupervised learning methods should be robust to various datasets. Here we pre-train models on COCO 2017 and compare with MoCo v2. Since COCO 2017 training set has only 118k images, we pre-train the models with 2000 epochs to have similar iterations with 200 epochs on ImageNet-1M. The results are shown in Tab. 6. For both MoCo v2 and DUPR, being pre-trained on COCO performs worse than on ImageNet. One possible reason is that the scale of COCO 2017 is much smaller than ImageNet-1M. But when pre-trained on COCO, DUPR consistently outperforms the MoCo v2.

4.7. Visualization of Spatial Sensitivity

To verify that patch Re-ID can learn spatial sensitive features, we visualize the relationship between IoU and similarity with ground truth box. We randomly select 1000 images from the ImageNet validation set. For each image, we sample 20 RoIs with different IoUs (range from 0 to 1) between the ground truth box and RoIs. We then apply the

pre-train	AP	AP ₅₀	AP ₇₅
random init.	33.8	60.2	33.1
super. IN-1M	53.5	81.3	58.8
MoCo v2 IN-1M	57.0 (+3.5)	82.4 (+1.1)	63.6 (+4.8)
DUPR IN-1M	58.5 (+5.0)	83.2 (+1.9)	65.2 (+6.4)
MoCo v2 COCO	55.2 (+1.7)	81.3 (+0.0)	61.3 (+2.5)
DUPR COCO	56.6 (+3.1)	81.8 (+0.5)	62.6 (+3.8)

Table 6. **Finetune object detection by representations pre-trained with different datasets.** We finetune Faster R-CNN R-50-C4 on trainval07+12 and test on test2007. The IN-1M denotes models pre-trained on ImageNet-1M while the COCO denotes models pre-trained on COCO 2017train.

pre-train	AP	AP ₅₀	AP ₇₅
random init.	24.5	39.0	25.7
supervised	37.4	56.5	39.7
InsDis [36]	35.5 (−1.9)	54.1 (−2.4)	38.2 (−1.5)
PIRL [29]	35.8 (−1.6)	54.3 (−2.2)	38.5 (−1.2)
SwAV [3]	35.2 (−2.2)	54.9 (−1.6)	37.6 (−2.1)
MoCo [17]	36.3 (−1.1)	55.0 (−1.5)	39.0 (−0.7)
MoCo v2 [5]	37.4 (+0.0)	56.5 (+0.0)	40.0 (+0.3)
DUPR (ours)	38.0 (+0.6)	57.2 (+0.7)	40.7 (+1.0)

(a) RetinaNet, R50-FPN, 1× schedule

pre-train	AP	AP ₅₀	AP ₇₅
random init.	32.2	49.4	34.2
supervised	38.9	58.5	41.5
InsDis [36]	38.0 (−0.9)	57.4 (−1.1)	40.5 (−1.0)
PIRL [29]	38.5 (−0.4)	57.7 (−0.8)	41.2 (−0.3)
SwAV [3]	38.6 (−0.3)	58.9 (+0.4)	41.1 (−0.4)
MoCo [17]	38.7 (−0.2)	57.9 (−0.6)	41.5 (+0.0)
MoCo v2 [5]	39.4 (+0.5)	59.0 (+0.5)	42.2 (+0.7)
DUPR (ours)	40.0 (+1.1)	59.6 (+1.1)	43.0 (+1.5)

(b) RetinaNet, R50-FPN, 2× schedule

Table 7. **Object detection of RetinaNet on COCO.** All the unsupervised models are pre-trained on ImageNet for 200 epochs. All the results are implemented by us in the same settings.

pre-train	Instance seg.		Semantic seg. mIoU
	AP ^{mk}	AP ₅₀ ^{mk}	
random init.	25.4	51.1	65.3
super. IN-1M	32.9	59.6	74.6
InstDis [36]	33.0 (+0.1)	60.1 (+0.5)	73.3 (−1.3)
PIRL [29]	33.9 (+1.0)	61.7 (+2.1)	74.6 (+0.0)
SwAV [3]	33.9 (+1.0)	62.4 (+2.8)	73.0 (+1.6)
MoCo [17]	32.3 (−0.6)	59.3 (−0.3)	75.3 (+0.7)
MoCo v2 [5]	33.9 (+1.0)	60.8 (+1.2)	75.7 (+1.1)
DUPR (ours)	34.4 (+1.5)	62.3 (+2.7)	76.6 (+2.0)

Table 8. **Results on Cityscapes.** Our method outperforms all other unsupervised and supervised counterparts.

RoI Align to ground truth box and each RoI to extract features from conv4_x feature map since it has a relatively large resolution. Denote the feature extracted from ground truth box as q and the feature extracted from RoI having α IoU with ground truth box as k_α . Both q and k_α are of shape (C, S, S) . We calculate the average of cosine similarity between q and k_α as:

$$Sim_{q,k_\alpha} = \frac{1}{S \times S} \sum q_{i,j} \cdot k_{\alpha,i,j}, \quad (8)$$



Figure 5. **The visualization of spatial sensitivity.** (a) We calculate the similarity between ground truth (Red bounding box) and RoIs (blue box with different IoUs) using the Eq. 8. (b) shows that DUPR learns more spatial sensitive features than MoCo v2. More specifically, DUPR have higher similarity between RoI and ground truth box when their IoU is larger than 0.5, and have smaller similarity than MoCo v2 when IoU is less than 0.3. It means that features learned by DUPR are more discriminative than MoCo v2 to suppress wrong predictions (boxes with small IoU).

where $q_{i,j}$ and $k_{\alpha,i,j}$ are normalized features at position (i, j) of region features. We compare DUPR with MoCo v2 in Fig. 5. This visualization shows that DUPR is more sensitive to IoU as DUPR has a higher slope compared to MoCo v2. When IoU between RoI and ground truth box is above 0.5 (usually assigned as positive samples in object detection [33]), DUPR has higher similarity. And when IoU is below 0.3 (usually assigned as negative samples), DUPR has a lower similarity. Such property makes the representations easy to surpass the false-negative RoIs.

4.8. Nearest Neighbors

We find the top-4 nearest neighbors using the normalized conv5_x feature map. In Fig. 6 we show the retrieval results using features learned by DUPR vs. MoCo v2. The results of MoCo v2 only care about the category information but are not aligned in spatial positions (local patch of images are not similar to the query images), while the results of DUPR align well in spatial position. This phenomenon is consistent with our patch Re-ID pretext task, which learns to match the same identity’s corresponding patch in the other view. See more retrieval results of KNN in our Appendix.

5. Conclusion

This paper presents a pretext task named patch Re-ID to pre-train representations in a deeply unsupervised style for object detectors. Our method can capture more spatial information and outperforms other unsupervised models and even the supervised counterpart when transferred to object detection. Moreover, our method is robust to various pre-training dataset, object detectors, finetuning time, and limited annotations. We hope our simple yet effective method could serve as a baseline of pre-training representations for object detection without labels.

Acknowledgement We thank Wenqi Shao for insightful discussions.

pre-train	AP ^{bb}	AP ^{bb} ₅₀	AP ^{bb} ₇₅	AP ^{mk}	AP ^{mk} ₅₀	AP ^{mk} ₇₅	AP ^{bb}	AP ^{bb} ₅₀	AP ^{bb} ₇₅	AP ^{mk}	AP ^{mk} ₅₀	AP ^{mk} ₇₅
random init.	31.0	49.5	33.2	28.5	46.8	30.4	26.4	44.0	27.8	29.3	46.9	30.8
supervised	38.9	59.6	42.7	35.4	56.5	38.1	38.2	58.2	41.2	33.3	54.7	35.2
InstDis [36]	37.5 (−1.4)	57.6 (−2.0)	40.6 (−2.1)	34.1 (−1.3)	54.7 (−1.8)	36.5 (−1.6)	37.8 (−0.4)	57.0 (−1.2)	41.0 (−0.2)	33.1 (−0.2)	54.2 (−0.5)	35.3 (+0.1)
PIRL [29]	37.6 (−1.3)	57.7 (−1.9)	41.1 (−1.6)	34.1 (−1.3)	54.7 (−1.8)	36.2 (−1.9)	37.4 (−0.8)	56.6 (−1.6)	40.3 (−0.9)	32.8 (−0.5)	53.4 (−1.3)	34.8 (−0.4)
SwAV [3]	38.6 (−0.3)	60.5 (+0.9)	41.5 (−1.2)	35.5 (+0.1)	57.1 (+0.6)	37.8 (−0.3)	33.0 (−5.2)	54.3 (−3.9)	34.6 (−6.6)	29.5 (−3.8)	50.4 (−4.3)	30.4 (−4.8)
MoCo [17]	38.5 (−0.4)	58.9 (−0.7)	42.0 (−0.7)	35.1 (−0.3)	55.9 (−0.6)	37.7 (−0.4)	38.5 (+0.3)	58.3 (+0.1)	41.6 (+0.4)	33.6 (+0.3)	54.8 (+0.1)	35.6 (+0.4)
MoCo v2 [5]	38.9 (+0.0)	59.4 (−0.2)	42.4 (−0.3)	35.5 (+0.1)	56.5 (+0.0)	38.2 (+0.1)	38.9 (+0.7)	58.5 (+0.3)	42.1 (+0.9)	34.2 (+0.9)	55.2 (+0.5)	36.6 (+1.4)
DUPR (ours)	40.0 (+1.1)	60.4 (+0.8)	43.4 (+0.7)	36.2 (+0.8)	57.6 (+1.1)	38.9 (+0.8)	39.6 (+1.4)	59.4 (+1.2)	42.8 (+1.6)	34.5 (+1.2)	55.9 (+1.2)	36.7 (+1.5)

(a) Mask R-CNN, R50-FPN, 1× schedule

pre-train	AP ^{bb}	AP ^{bb} ₅₀	AP ^{bb} ₇₅	AP ^{mk}	AP ^{mk} ₅₀	AP ^{mk} ₇₅	AP ^{bb}	AP ^{bb} ₅₀	AP ^{bb} ₇₅	AP ^{mk}	AP ^{mk} ₅₀	AP ^{mk} ₇₅
random init.	36.7	56.7	40.0	33.7	53.8	35.9	35.6	54.6	38.2	31.4	51.5	33.5
supervised	40.6	61.3	44.4	36.8	58.1	39.5	40.0	59.9	43.1	34.7	56.5	36.9
MoCo [17]	40.8 (+0.2)	61.6 (+0.3)	44.7 (+0.3)	36.9 (+0.1)	58.4 (+0.3)	39.7 (+0.2)	40.7 (+0.7)	60.5 (+0.6)	44.1 (+1.0)	35.4 (+0.7)	57.3 (+0.8)	37.6 (+0.7)
MoCo v2 [5]	40.9 (+0.3)	61.5 (+0.2)	44.7 (+0.3)	37.0 (+0.2)	58.7 (+0.6)	39.8 (+0.4)	41.0 (+1.0)	60.5 (+0.6)	44.5 (+1.4)	35.7 (+1.0)	57.3 (+0.8)	38.1 (+1.2)
DUPR (ours)	41.6 (+1.0)	62.3 (+1.0)	45.2 (+0.8)	37.5 (+0.7)	59.2 (+1.1)	40.2 (+0.7)	41.3 (+1.3)	61.2 (+1.3)	45.0 (+1.9)	35.9 (+1.2)	57.7 (+1.2)	38.4 (+1.5)

(b) Mask R-CNN, R50-C4, 1× schedule

(c) Mask R-CNN, R50-FPN, 2× schedule

pre-train	AP ^{bb}	AP ^{bb} ₅₀	AP ^{bb} ₇₅	AP ^{mk}	AP ^{mk} ₅₀	AP ^{mk} ₇₅	AP ^{bb}	AP ^{bb} ₅₀	AP ^{bb} ₇₅	AP ^{mk}	AP ^{mk} ₅₀	AP ^{mk} ₇₅
random init.	2.5	5.5	1.9	2.2	4.6	1.9	18.8	33.2	19.2	17.6	30.6	17.9
supervised	11.5	22.0	10.8	11.1	20.6	10.6	24.2	40.2	25.6	22.4	37.5	23.3
MoCo v2 [5]	9.3 (−2.2)	17.0 (−5.0)	9.1 (−1.7)	8.8 (−2.3)	15.8 (−4.8)	8.6 (−2.0)	24.9 (+0.7)	40.6 (+0.4)	26.5 (+0.9)	22.9 (+0.5)	38.1 (+0.6)	24.1 (+0.8)
DUPR (ours)	11.4 (−0.1)	21.0 (−1.0)	11.3 (+0.5)	10.9 (−0.2)	19.7 (−0.9)	10.8 (+0.2)	25.5 (+1.3)	41.1 (+0.9)	27.2 (+1.6)	23.4 (+1.0)	38.8 (+1.3)	24.6 (+1.3)

(d) Mask R-CNN, R50-C4, 2× schedule

Table 9. **Object detection and instance segmentation finetuned on COCO.** All the compared methods are pre-trained for 200 epochs on ImageNet. The results of random init, supervised, and MoCo are from [17]. We implement other methods following the same settings.

pre-train	AP ^{bb}	AP ^{bb} ₅₀	AP ^{bb} ₇₅	AP ^{mk}	AP ^{mk} ₅₀	AP ^{mk} ₇₅	AP ^{bb}	AP ^{bb} ₅₀	AP ^{bb} ₇₅	AP ^{mk}	AP ^{mk} ₅₀	AP ^{mk} ₇₅
random init.	2.5	5.5	1.9	2.2	4.6	1.9	18.8	33.2	19.2	17.6	30.6	17.9
supervised	11.5	22.0	10.8	11.1	20.6	10.6	24.2	40.2	25.6	22.4	37.5	23.3
MoCo v2 [5]	9.3 (−2.2)	17.0 (−5.0)	9.1 (−1.7)	8.8 (−2.3)	15.8 (−4.8)	8.6 (−2.0)	24.9 (+0.7)	40.6 (+0.4)	26.5 (+0.9)	22.9 (+0.5)	38.1 (+0.6)	24.1 (+0.8)
DUPR (ours)	11.4 (−0.1)	21.0 (−1.0)	11.3 (+0.5)	10.9 (−0.2)	19.7 (−0.9)	10.8 (+0.2)	25.5 (+1.3)	41.1 (+0.9)	27.2 (+1.6)	23.4 (+1.0)	38.8 (+1.3)	24.6 (+1.3)

(a) Mask R-CNN, R50-FPN, COCO-1%

(b) Mask R-CNN, R50-FPN, COCO-10%

Table 10. **Semi-supervised object detection and instance segmentation finetuned on COCO.** We finetune the Mask R-CNN R-50-FPN on COCO with only 1% and 10% annotations.

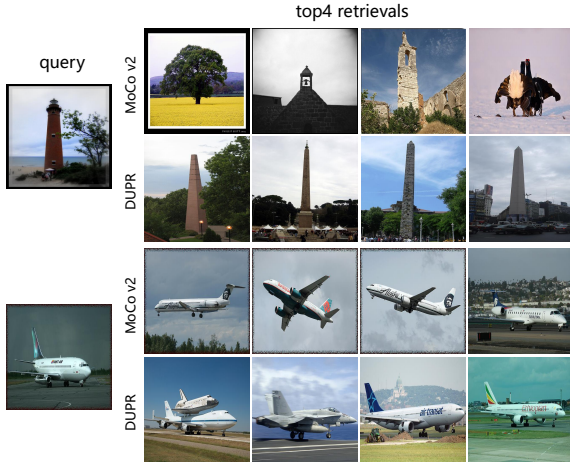


Figure 6. **Top-4 nearest-neighbor retrieval results.** Our model’s retrieval results are more close to the query image in spatially related information (width of the tower and pose of the plane).

6. Appendix

6.1. More Experiments

Pre-training with 800 epochs. We pre-train DUPR with 800 epochs and compare it with MoCo v2 in Tab. 11. Pre-training DUPR with 800 epochs consistently outperforms MoCo v2 with 800 epochs.

Mask AP of Mask R-CNN R-50-FPN at different iterations. In our main paper, we present the box AP for Mask R-CNN R-50-FPN at different iterations. Here we show the mask AP for Mask R-CNN R-50-FPN in Fig. 7.

6.2. More visualization results

KNN retrieval results We show more qualitative retrieval results of KNN in Fig. 8. The retrieval results in red boxes have different categories with the query images, while the retrieval results in yellow boxes have the correct categories but are not aligned well with the query images. DUPR provides a fine-grained matching (each local patch of retrieval results is closer to the corresponding patch in the query image). For example, the retrieval results of DUPR capture pose better than the retrieval results of MoCo v2, as shown in Fig. 8.

Affinity between RoI features in two views We visualize the affinity matrix between the RoI features of the same identity in two views. First, we create two views by random augmentations (including color jitter, gaussian blur, grayscale, and random crop) while keep the ground truth bounding box not cut off. Then we resize the images to 448. For each view, we apply an RoI Align on top of conv5_x feature map to extract the feature from the ground truth bounding box (green box in Fig. 9). The output feature shape of RoI Align is (2048, 14, 14). The RoI features can be re-

pre-train	epoch	AP ₅₀	AP	AP ₇₅
random init.	-	60.2	33.8	33.1
supervised	100	81.3	53.5	58.8
MoCo v1 [17]	200	81.5 (+0.2)	55.9 (+2.4)	62.6 (+3.8)
MoCo v2 [5]	200	82.4 (+1.1)	57.0 (+3.5)	63.6 (+4.8)
MoCo v2 [5]	800	82.5 (+1.2)	57.4 (+3.9)	64.0 (+5.2)
DUPR	200	83.2 (+1.9)	58.5 (+5.0)	65.2 (+6.4)
DUPR	800	83.3 (+2.0)	59.1 (+5.6)	66.2 (+7.4)

Table 11. **Object detection on PASCAL VOC.** All the models are pre-trained on ImageNet. We finetune the Faster R-CNN R-50-C4 on Pascal VOC trainval07+12 and evaluated on test2007. Pre-training DUPR with 800 epochs consistently improves the performance. DUPR 800 epochs outperforms the MoCo v2 800 epochs by **1.7 points** in AP.

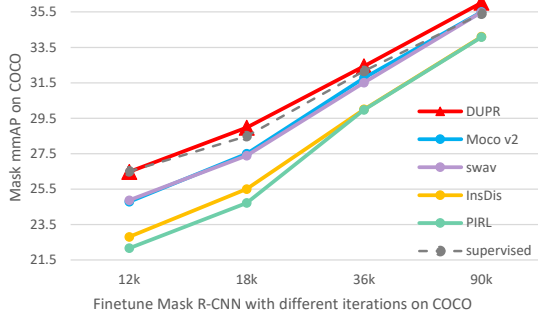


Figure 7. **Mask mAP of finetuning Mask R-CNN R-50-FPN on COCO at different iterations.** All the reported unsupervised models are pre-trained on the ImageNet-1M training set with 200 epochs. DUPR outperforms all other unsupervised methods and even the supervised counterpart. When finetuning the Mask R-CNN with 12k iterations, DUPR outperforms the MoCo v2 by **1.7 points** in mask mAP.

shaped to be (2048, 196). The affinity matrix is calculated between two RoI features as:

$$\mathcal{A}_{i,j} = \frac{\exp(\text{sim}(f_{1,i}, f_{2,j})/\tau)}{\sum_k \exp(\text{sim}(f_{1,k}, f_{2,j})/\tau)} \quad (9)$$

where $f_1 \in \mathcal{R}^{2048 \times 196}$ and $f_2 \in \mathcal{R}^{2048 \times 196}$ are two vectorized RoI features. $f_{1,i} \in \mathcal{R}^{2048}$ and $f_{2,j} \in \mathcal{R}^{2048}$ are i -th and j -th point feature of two RoI features. For visualization, we set $\tau = 0.001$. We visualize the affinity matrix in Fig. 9. The ideal affinity matrix is the identity matrix. The results show that the encoder pre-trained with DUPR has a better affinity matrix than the MoCo v2, which indicates that DUPR encodes more information to match the correspondence patches.

Matching between two views We use the learned representations to calculate the keypoints matching between two views. First, we create two views via random data augmentation following the settings in [17]. We set the image size to 448. We use the feature map of conv4_x (which is of shape (1024, 28, 28)) for matching. For each patch (one of

28×28) feature in one view, we find the patch with the highest similarity in the other view. For visualization, we use the point to represent a patch. The results shown in Fig. 10 demonstrate that DUPR matches the corresponding patches better than MoCo v2.

6.3. More Implementation Details

All the algorithms of object detection, instance segmentation, and semantic segmentation are implemented in detectron2³. For Mask R-CNN R-50-FPN, Mask R-CNN R-50-C4, and Faster R-CNN-C4, we follow the settings in MoCo [17]. For RetinaNet R-50-FPN, we also add an extra normalization layer similar to Mask R-CNN R-50-FPN in MoCo [17]. The pre-trained weights of PIRL [29], InsDis [36] are downloaded from Pycontrast⁴. The pre-trained weights of SwAV is downloaded from the official code⁵.

References

- [1] Philip Bachman, R Devon Hjelm, and William Buchwalter. Learning representations by maximizing mutual information across views. In *Advances in Neural Information Processing Systems*, pages 15535–15545, 2019.
- [2] Mathilde Caron, Piotr Bojanowski, Armand Joulin, and Matthijs Douze. Deep clustering for unsupervised learning of visual features. In *Proceedings of the European Conference on Computer Vision (ECCV)*, pages 132–149, 2018.
- [3] Mathilde Caron, Ishan Misra, Julien Mairal, Priya Goyal, Piotr Bojanowski, and Armand Joulin. Unsupervised learning of visual features by contrasting cluster assignments. *arXiv preprint arXiv:2006.09882*, 2020.
- [4] Ting Chen, Simon Kornblith, Mohammad Norouzi, and Geoffrey Hinton. A simple framework for contrastive learning of visual representations. *arXiv preprint arXiv:2002.05709*, 2020.
- [5] Xinlei Chen, Haoqi Fan, Ross Girshick, and Kaiming He. Improved baselines with momentum contrastive learning. *arXiv preprint arXiv:2003.04297*, 2020.
- [6] Jifeng Dai, Yi Li, Kaiming He, and Jian Sun. R-fcn: Object detection via region-based fully convolutional networks. *arXiv preprint arXiv:1605.06409*, 2016.
- [7] Carl Doersch, Abhinav Gupta, and Alexei A Efros. Unsupervised visual representation learning by context prediction. In *Proceedings of the IEEE international conference on computer vision*, pages 1422–1430, 2015.
- [8] Carl Doersch and Andrew Zisserman. Multi-task self-supervised visual learning. In *Proceedings of the IEEE International Conference on Computer Vision*, pages 2051–2060, 2017.
- [9] Jeff Donahue and Karen Simonyan. Large scale adversarial representation learning. In *Advances in Neural Information Processing Systems*, pages 10542–10552, 2019.

³<https://github.com/facebookresearch/detectron2>

⁴<https://github.com/HobbitLong/PyContrast>

⁵<https://github.com/facebookresearch/swav>

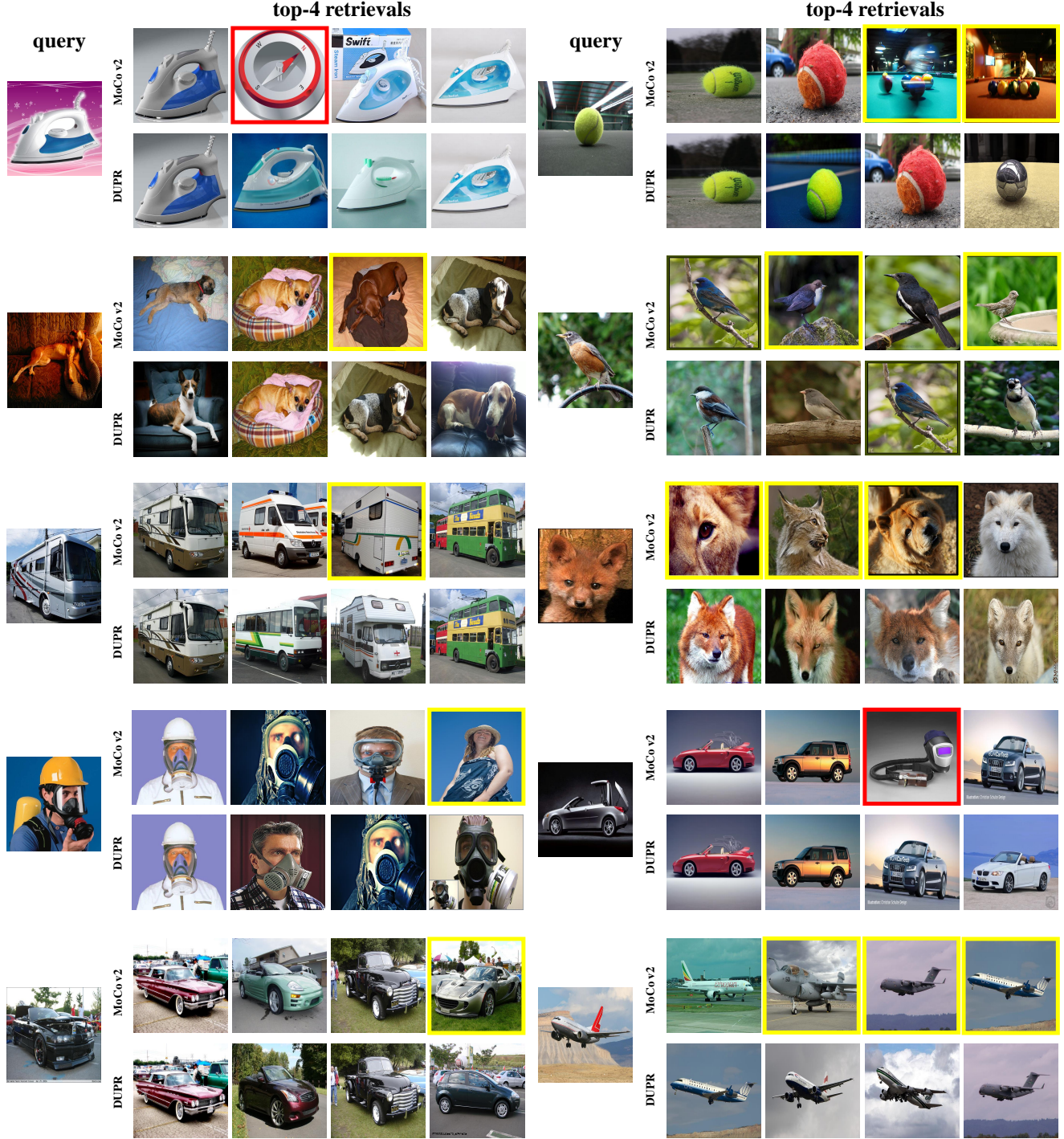


Figure 8. **Top-4 nearest-neighbor retrieval results.** The retrieval results in red boxes have the wrong categories. The retrieval results in yellow boxes have the correct categories but are not aligned well with the query images. The retrieval results of DUPR are more close to the query images.

- [10] Spyros Gidaris, Andrei Bursuc, Nikos Komodakis, Patrick Pérez, and Matthieu Cord. Learning representations by predicting bags of visual words. In *Proceedings of the IEEE/CVF Conference on Computer Vision and Pattern Recognition*, pages 6928–6938, 2020.

- [11] Spyros Gidaris, Praveer Singh, and Nikos Komodakis. Un-supervised representation learning by predicting image rotations. *arXiv preprint arXiv:1803.07728*, 2018.

- [12] Ross Girshick, Jeff Donahue, Trevor Darrell, and Jitendra Malik. Rich feature hierarchies for accurate object detection

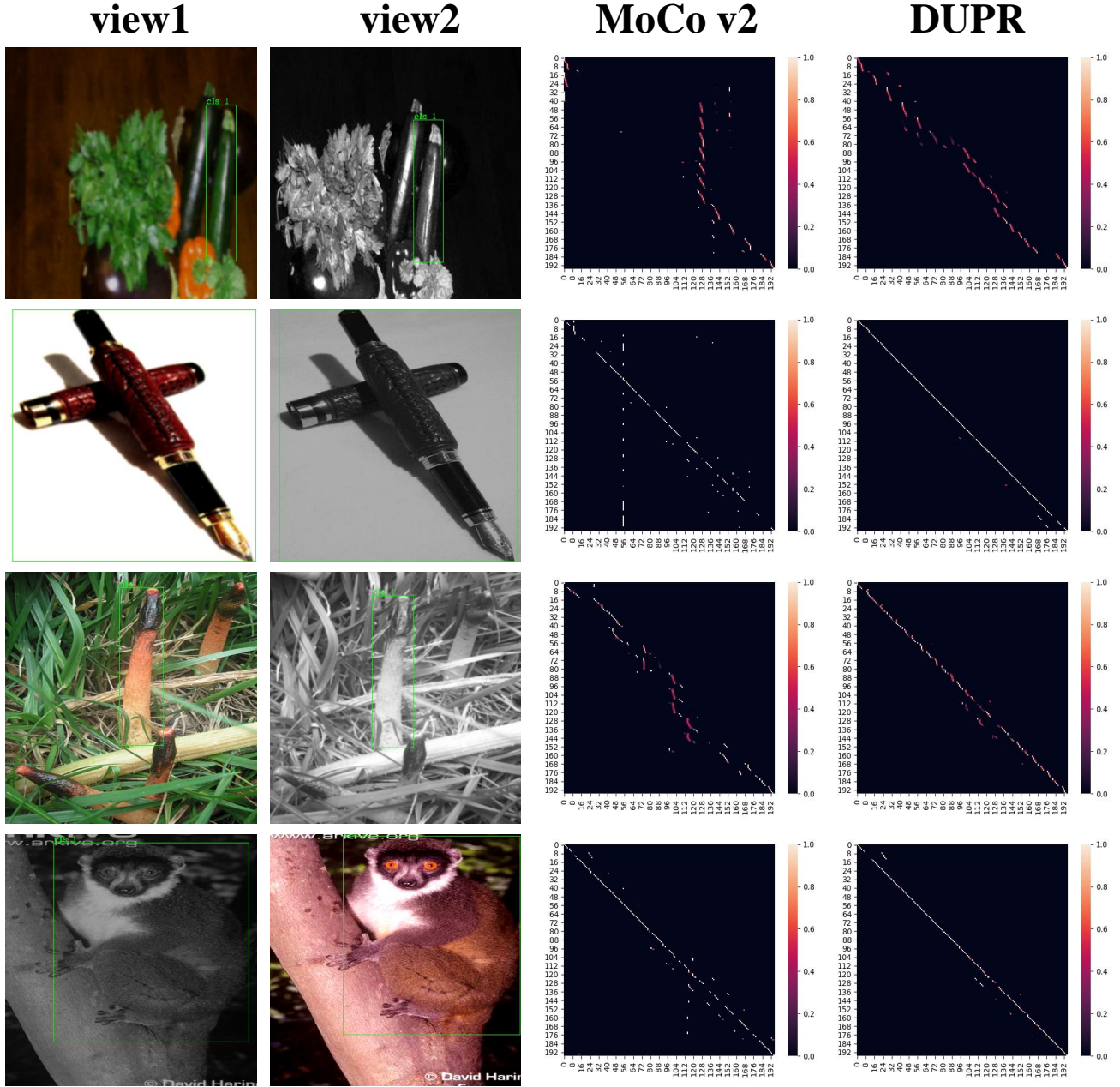


Figure 9. Comparison of affinity matrix between MoCo v2 and DUPR in the ground truth bounding box of two views. The green box denotes the ground truth bounding box. The right pictures show the affinity matrix of MoCo v2 and DUPR. The ideal affinity matrix is the identity matrix.

and semantic segmentation. In *Proceedings of the IEEE conference on computer vision and pattern recognition*, pages 580–587, 2014.

- [13] Ian Goodfellow, Jean Pouget-Abadie, Mehdi Mirza, Bing Xu, David Warde-Farley, Sherjil Ozair, Aaron Courville, and Yoshua Bengio. Generative adversarial nets. In *Advances in neural information processing systems*, pages 2672–2680, 2014.
- [14] Jean-Bastien Grill, Florian Strub, Florent Altché, Corentin

Tallec, Pierre H Richemond, Elena Buchatskaya, Carl Doersch, Bernardo Avila Pires, Zhaohan Daniel Guo, Mohammad Gheshlaghi Azar, et al. Bootstrap your own latent: A new approach to self-supervised learning. *arXiv preprint arXiv:2006.07733*, 2020.

- [15] Raia Hadsell, Sumit Chopra, and Yann LeCun. Dimensionality reduction by learning an invariant mapping. In *2006 IEEE Computer Society Conference on Computer Vision and Pattern Recognition (CVPR’06)*, volume 2, pages 1735–1742.

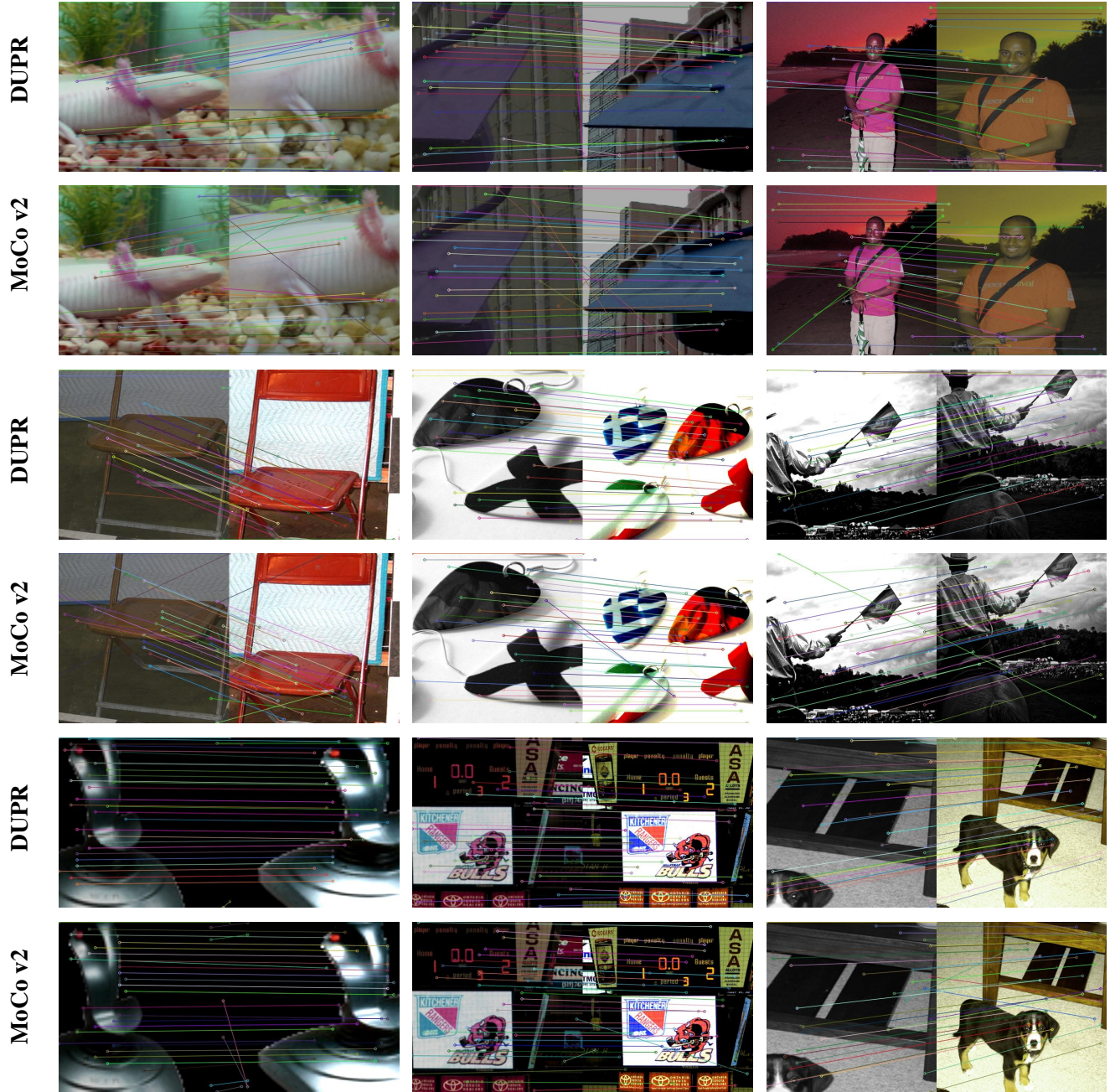


Figure 10. **Visualiztion of matching in two views.** We use the learned representations from DUPR and MoCo v2 to match the corresponding patches in two views. Each image is split into 28×28 patches. For visualization, we use points to represent patches. It shows that DUPR can match the local patches in the other view better than MoCo v2.

IEEE, 2006.

- [16] Tengda Han, Weidi Xie, and Andrew Zisserman. Video representation learning by dense predictive coding. In *Proceedings of the IEEE International Conference on Computer Vision Workshops*, pages 0–0, 2019.
- [17] Kaiming He, Haoqi Fan, Yuxin Wu, Saining Xie, and Ross Girshick. Momentum contrast for unsupervised visual representation learning. In *Proceedings of the IEEE/CVF Conference on Computer Vision and Pattern Recognition*, pages

9729–9738, 2020.

- [18] Kaiming He, Georgia Gkioxari, Piotr Dollár, and Ross Girshick. Mask r-cnn. In *Proceedings of the IEEE international conference on computer vision*, pages 2961–2969, 2017.
- [19] Kaiming He, Xiangyu Zhang, Shaoqing Ren, and Jian Sun. Deep residual learning for image recognition. In *Proceedings of the IEEE conference on computer vision and pattern recognition*, pages 770–778, 2016.
- [20] Olivier J Hénaff, Aravind Srinivas, Jeffrey De Fauw, Ali

- Razavi, Carl Doersch, SM Eslami, and Aaron van den Oord. Data-efficient image recognition with contrastive predictive coding. *arXiv preprint arXiv:1905.09272*, 2019.
- [21] Geoffrey E Hinton and Richard S Zemel. Autoencoders, minimum description length and helmholtz free energy. In *Advances in neural information processing systems*, pages 3–10, 1994.
- [22] R Devon Hjelm, Alex Fedorov, Samuel Lavoie-Marchildon, Karan Grewal, Phil Bachman, Adam Trischler, and Yoshua Bengio. Learning deep representations by mutual information estimation and maximization. *arXiv preprint arXiv:1808.06670*, 2018.
- [23] Md Amirul Islam, Sen Jia, and Neil DB Bruce. How much position information do convolutional neural networks encode? *arXiv preprint arXiv:2001.08248*, 2020.
- [24] Chen-Yu Lee, Saining Xie, Patrick Gallagher, Zhengyou Zhang, and Zhuowen Tu. Deeply-supervised nets. In *Artificial intelligence and statistics*, pages 562–570, 2015.
- [25] Tsung-Yi Lin, Piotr Dollár, Ross Girshick, Kaiming He, Bharath Hariharan, and Serge Belongie. Feature pyramid networks for object detection. In *Proceedings of the IEEE conference on computer vision and pattern recognition*, pages 2117–2125, 2017.
- [26] Tsung-Yi Lin, Priya Goyal, Ross Girshick, Kaiming He, and Piotr Dollár. Focal loss for dense object detection. In *Proceedings of the IEEE international conference on computer vision*, pages 2980–2988, 2017.
- [27] Shu Liu, Lu Qi, Haifang Qin, Jianping Shi, and Jiaya Jia. Path aggregation network for instance segmentation. In *Proceedings of the IEEE conference on computer vision and pattern recognition*, pages 8759–8768, 2018.
- [28] Wei Liu, Dragomir Anguelov, Dumitru Erhan, Christian Szegedy, Scott Reed, Cheng-Yang Fu, and Alexander C Berg. Ssd: Single shot multibox detector. In *European conference on computer vision*, pages 21–37. Springer, 2016.
- [29] Ishan Misra and Laurens van der Maaten. Self-supervised learning of pretext-invariant representations. In *Proceedings of the IEEE/CVF Conference on Computer Vision and Pattern Recognition*, pages 6707–6717, 2020.
- [30] Mehdi Noroozi and Paolo Favaro. Unsupervised learning of visual representations by solving jigsaw puzzles. In *European Conference on Computer Vision*, pages 69–84. Springer, 2016.
- [31] Aaron van den Oord, Yazhe Li, and Oriol Vinyals. Representation learning with contrastive predictive coding. *arXiv preprint arXiv:1807.03748*, 2018.
- [32] Joseph Redmon, Santosh Divvala, Ross Girshick, and Ali Farhadi. You only look once: Unified, real-time object detection. In *Proceedings of the IEEE conference on computer vision and pattern recognition*, pages 779–788, 2016.
- [33] Shaoqing Ren, Kaiming He, Ross Girshick, and Jian Sun. Faster r-cnn: Towards real-time object detection with region proposal networks. In *Advances in neural information processing systems*, pages 91–99, 2015.
- [34] Yonglong Tian, Dilip Krishnan, and Phillip Isola. Contrastive multiview coding. *arXiv preprint arXiv:1906.05849*, 2019.
- [35] Zhi Tian, Chunhua Shen, Hao Chen, and Tong He. Fcos: Fully convolutional one-stage object detection. In *Proceedings of the IEEE international conference on computer vision*, pages 9627–9636, 2019.
- [36] Zhirong Wu, Yuanjun Xiong, Stella X Yu, and Dahua Lin. Unsupervised feature learning via non-parametric instance discrimination. In *Proceedings of the IEEE Conference on Computer Vision and Pattern Recognition*, pages 3733–3742, 2018.
- [37] Saining Xie and Zhuowen Tu. Holistically-nested edge detection. In *Proceedings of the IEEE international conference on computer vision*, pages 1395–1403, 2015.
- [38] Richard Zhang, Phillip Isola, and Alexei A Efros. Colorful image colorization. In *European conference on computer vision*, pages 649–666. Springer, 2016.
- [39] Richard Zhang, Phillip Isola, and Alexei A Efros. Split-brain autoencoders: Unsupervised learning by cross-channel prediction. In *Proceedings of the IEEE Conference on Computer Vision and Pattern Recognition*, pages 1058–1067, 2017.
- [40] Hengshuang Zhao, Jianping Shi, Xiaojuan Qi, Xiaogang Wang, and Jiaya Jia. Pyramid scene parsing network. In *Proceedings of the IEEE conference on computer vision and pattern recognition*, pages 2881–2890, 2017.
- [41] Chengxu Zhuang, Alex Lin Zhai, and Daniel Yamins. Local aggregation for unsupervised learning of visual embeddings. In *Proceedings of the IEEE International Conference on Computer Vision*, pages 6002–6012, 2019.